Exosomes derived from impaired liver aggravate alveolar bone loss via shuttle of Fasn in type 2 diabetes mellitus

Jiani Liu [a],[1], Geng Dou [b],[1], Wanmin Zhao [b],[1], Ji'an Hu [a], Zhiwei Jiang [a], Wenzhe Wang [b], Hanzhe Wang [b], Shiyu Liu [b], Yan Jin [b], Yimin Zhao [b],[***], Qianming Chen [a],[**], Bei Li [b],[*]

[a] Stomatology Hospital, School of Stomatology, Zhejiang University School of Medicine, Zhejiang Provincial Clinical Research Center for Oral Diseases, Key Laboratory of Oral Biomedical Research of Zhejiang Province, Cancer Center of Zhejiang University, Hangzhou, 310006, China
[b] State Key Laboratory of Oral & Maxillofacial Reconstruction and Regeneration, National Clinical Research Center for Oral Diseases, Shaanxi International Joint Research Center for Oral Diseases, Center for Tissue Engineering, School of Stomatology, The Fourth Military Medical University, Xi'an, Shaanxi, 710032, China

ARTICLE INFO

ABSTRACT

Type 2 diabetes mellitus (T2DM) exacerbates irreversible bone loss in periodontitis, but the mechanism of impaired bone regeneration caused by the abnormal metabolic process of T2DM remains unclear. Exosomes are regarded as the critical mediator in diabetic impairment of regeneration via organ or tissue communication. Here, we find that abnormally elevated exosomes derived from metabolically impaired liver in T2DM are significantly enriched in the periodontal region and induced pyroptosis of periodontal ligament cells (PDLCs). Mechanistically, fatty acid synthase (Fasn), the main differentially expressed molecule in diabetic exosomes results in ectopic fatty acid synthesis in PDLCs and activates the cleavage of gasdermin D. Depletion of liver Fasn effectively mitigates pyroptosis of PDLCs and alleviates bone loss. Our findings elucidate the mechanism of exacerbated bone loss in diabetic periodontitis and reveal the exosome-mediated organ communication in the "liver-bone" axis, which shed light on the prevention and treatment of diabetic bone disorders in the future.

1. Introduction

Type 2 diabetes mellitus (T2DM) is a chronic condition characterized by hyperglycemia and systemic metabolic disorders, which seriously interfere with the tissue healing process represented by bone and skin [1,2]. The clinical association of T2DM and periodontitis has been well established, including exacerbated alveolar bone loss and diminished bone formation [3,4]. Studies suggested that individuals with diabetes mellitus and periodontitis experience a "two-hit" effect, in which the presence of periodontitis exacerbates inflammation and hinders repair mechanisms, leading to accelerated and severe periodontal destruction [5,6]. Accordingly, diabetic periodontitis lacks standardized and long-term management with a relatively poor prognosis in clinical practice [7].

A newly identified form of necrotic cell death modality called pyroptosis has been found to exacerbate inflammatory processes in periodontitis [8]. Gasdermin D (GSDMD)-driven pyroptosis plays a pivotal role of destroyer in the pathogenesis of periodontitis via inhibiting osteogenesis and promoting osteoclast differentiation to induce progressive bone loss [9,10]. There are a large group of mesenchymal cells in periodontal ligament, which are dedicated to the periodontal bone regeneration [11]. The harsh periodontal microenvironment caused by diabetic metabolic disorder exerts a deleterious impact on periodontal ligament cells (PDLCs). Hence, it is worth exploring and revealing whether the abnormal metabolic process of T2DM exacerbates bone destruction via pyroptosis.

Extracellular vesicles (EVs), particularly exosomes, have garnered increasing interest in the field of metabolic diseases, including T2DM [12]. Exosomes are small lipid bilayer vesicles released by cells into circulation [13,14], which can transfer functional cargo, such as lipids, proteins, and nucleic acids, to neighbouring or distant cells and tissues [15]. Elevated levels of circulating exosomes in patients with T2DM

---

have been observed to exert adverse effects on tissue regeneration, such as hindering wound healing [16,17], as well as impairing insulin action in skeletal muscle [18]. Emerging studies demonstrated that circulating exosomes mediated inter-organ or inter-tissue communication in diabetes or obesity [19,20]. Therefore, it is plausible that circulating exosomes contribute to impaired bone regeneration in periodontitis in the context of T2DM. As a central metabolic site, the liver plays a critical role in regulating bone homeostasis through liver-bone crosstalk [21]. For instance, taurine synthesis induced by vitamin B12 in liver regulate bone development via GH/IGF1 pathway [22]. Similarly, insulin-like growth factor binding protein 1 (IGFB1) produced by liver affects bone resorption by binding to integrin-β1 on the surface of osteoclasts [23]. T2DM, a chronic metabolic disorder, is closely associated with various liver injuries, such as hepatic fibrosis, cirrhosis, non-alcoholic fatty liver disease (NAFLD) and non-alcoholic steatohepatitis (NASH), which further contribute to the progression of inflammatory damage in the body [24]. Liver-derived EVs in T2DM directly impair insulin sensitivity, inhibit glucose tolerance and promote endothelial inflammation [25,26]. The content and distribution of EVs released by the damaged liver are significantly altered, thus being proposed as a novel intercellular communication mode in systemic metabolic regulation [14, 27]. Taken together, these findings suggest a potentially novel paradigm existed in diabetic periodontitis that exosomes mediate the communication between liver and alveolar bone.

In this study, we found that T2DM contributed to pyroptosis of PDLCs which exacerbated periodontal bone loss via circulating exosomes. Circulating exosomes in T2DM mainly derived from impaired liver significantly accumulated in the periodontal region and fatty acid synthase (Fasn) transferred by exosomes resulted in ectopic synthesis of fatty acids, further inducing pyroptosis of PDLCs. Notably, inhibition of liver-derived exosomes and Fasn by genetic or pharmacological means significantly prevented cell pyroptosis and mitigated periodontal bone loss. This study proposes a new relationship between diabetes and periodontitis with a focus on an unrecognized mechanism of exosome-mediated interaction in liver-bone axis. Abnormal lipid metabolism caused by exosomes released from damaged liver leads to bone destruction, which explains a new mechanism of bone regeneration disorder in pathological state and enriches the specific communication pathway of the liver-bone axis. These findings also highlight the central role of Fasn-induced pyroptosis in weakened bone formation caused by diabetes, which provide advanced strategies for the prevention and treatment of diabetic bone disorder.

2. Experimental section

2.1. Materials and antibody

Propidium iodide solution (40710ES03), Alizarin red solution (60504ES25), DiR (40757ES25), DiI (40726ES10), FITC-Phalloidin (40735ES75) and Cell Counting Kit (CCK8) (40203ES60) were obtained from Yeasen (Shanghai, China). Hoechst 33258 (23491-45-4), β-glycerophosphate (G9422), Vitamin C (V-047) and dexamethasone (D4902) were obtained from Sigma-Aldrich (St.Louis, USA). TUNEL detection kit (C1088), DAB substrate kit (P0202), goat serum (C0265) and RIPA lysis buffer (P0013B) was obtained from Beyotime (Shanghai, China). GW4869 (HY-19363), palmitic acid (HY-N0830), stearic acid (HY–B2219) and C75 (HY-12364) were obtained from MedChemExpress (New Jersey, USA). Recombinant tumor necrosis factor-α (TNF-α) (300-01A) was obtained from Peprotech (Rocky Hill, USA). Sirius red (G1472), Penicillin/streptomycin (P1400), Oil red O (G1261), Decalcifying solution (E1171) and D-fluorescein (D8390) were obtained from Solarbio (Beijing, China). BCA protein assay kit (PA115) was obtained from TIANGEN (Beijing, China). Ultra EV isolation kit (EQULTRA-20A-1) was obtained from System biosciences (California, USA). Phosphate buffered solution (10010023), α-modified eagle medium (α-MEM) (12561056), trypsin-EDTA (25200072), type I collagenase (17018029),

fetal bovine serum (FBS) (10091148) were obtained from Gibco (New York, USA).

Alix (92880s) was obtained from Cell Signaling Technology. CD63 (sc-5275), GM130 (sc-55591), GSDMDN-AF594 (sc-393581), ASGPR (sc-166633, sc-52623), CD90-AF488 (sc-53456) and Fasn (sc-48357) were obtained from Santa Cruz Biotechnology. GSDMD (ab219800), HMGB1 (ab79823), Osteocalcin (ab93876), NLRP3 (ab263899, ab270449), TSG101 (ab125011), Calnexin (ab22595), anti-Cytochrome P450 2E1 (CYP2E1) (ab28146), Rab27a (ab55667), Adiponectin (ab181281) and PDX1 (ab134150) were obtained from Abcam. Albumin (NBPI-32458) was obtained from Novus. APC anti-human CD19 antibody (302212), PE anti-human CD34 antibody (343506), PE anti-human CD45 antibody (304058), FITC anti-human CD73 antibody (344015), PE anti-human CD90 antibody (328110), PE anti-human CD105 antibody (800504), APC anti-mouse CD63 antibody (143905) and PE anti-mouse CD81 antibody (104905) were obtained from Bio-Legend. The 10-nm gold-conjugated secondary antibody (anti-rabbit, 25108; anti-mouse, 25128) was obtained from Electron Microscopy Sciences (Pennsylvania, USA).

2.2. Cell culture

The experimental protocols were approved by the Hospital Ethics Committee (No. IRB-REV-2018020). Consent forms were obtained before conducting this research project. Teeth were extracted at the department of Oral and Maxillofacial Surgery, School of Stomatology, Fourth Military Medical University. The healthy PDLCs (H-PDLCs) were obtained from premolars extracted for orthodontic purposes or third molars extracted for impaction. The periodontitis PDLCs (P-PDLCs) were obtained from permanent teeth extracted due to periodontal disease. The diabetic periodontitis group (DPD-PDLCs) was obtained from patients with a history of diabetes who required tooth extraction due to periodontitis. The participants' ages vary from 20 to 40 years old, donor information was listed in Table S1. The participants were confirmed to be type 2 diabetes mellitus and the blood glucose level was controlled within the clinically acceptable range, extraction of teeth was reasonable and performed under the close supervision of the maxillofacial surgeon. After washing the collected teeth with cold PBS, the periodontal ligament tissue from the apical one-third was scraped off with a sterile blade, suspended in culture medium, and then centrifuged at 800 rpm for 5 min. After discarding the supernatant, collagenase I was added to digest the tissue fragments for 1 h. The tissue fragments were then resuspended in α-MEM medium supplemented with 10 % FBS and seeded in a 6-well plate. The expression markers of PDLCs were detected by flow cytometry. The 3rd to 5th generation of PDLCs were used in this study.

To simulate inflammation in vitro, TNF-α (10 μg mL^{-1}) was added to the culture medium of H-PDLCs. To apply exosomes stimulation in vitro, the quantified exosomes (50 μg mL^{-1}) were added to the cell culture medium. C75 solution (25 μmol L^{-1}) was added into medium for 2 h before treatment with exosomes. Palmitic acid (300 μmol L^{-1}) and stearic acid (300 μmol L^{-1}) were added to the PDLCs for 24 h. The cell viability was determined by CCK8 assay.

2.3. Osteogenic induction

The osteogenic capacity of PDLCs was evaluated by Alizarin red staining. After the treatment in different groups, the cells were incubated with osteogenic induction medium (α-MEM containing 10 % exosome-free FBS, 1 % penicillin/streptomycin, 5 mM β-glycerophosphate, 50 μg mL^{-1} vitamin C and 10 nM dexamethasone). The cells were cultured for 28 days, and the Alizarin red staining was performed according to the manufacturer's instructions. Specifically, the cells were fixed with isopropyl alcohol for 5 min and stained with Alizarin red solution for 10 s. Then, deionized water was used for cleaning the excess dye solution. After drying, photos were taken in the bright field. The

quantitative analysis was conducted by dissolution with 10 % cetyl-pyridinium chloride, and the OD value at 562 nm was measured.

2.4. Immunofluorescence

The cells after different treatments were fixed for the cellular immunofluorescence staining. After fixation, the tissue was decalcified and dehydrated, then prepared for OCT-embedded frozen sections. Then, the samples were washed with PBS for three times and permeated with 0.1 % Triton X-100 for 15 min. After blocking with the goat serum for 30 min, the samples were incubated with the primary antibody at 4 °C overnight. The excessive primary antibody was washed with PBS for three times, the samples were incubated with fluorescent secondary antibody. Finally, the nucleus was counterstained with Hoechst. The samples were observed and imaged under a confocal microscope (Nikon A1+, Japan). The fluorescence data analysis was performed by Image J.

2.5. Exosome isolation and characterization

The exosomes derived from serum was isolated by differential centrifugation. The serum was first centrifuged at 800 g for 5 min and 16,000 g for 30 min to remove the debris. Then, the supernatant was collected to ultracentrifuge at 4 °C for 70 min at 100,000 g. The precipitation at the bottom of the tube was washed with PBS and purified by ultracentrifugation once at 100,000 g for 70 min. Exosomes at the bottom of the tube was dissolved by PBS. The concentration was determined by a BCA kit. The size of exosomes was measured by nanoparticle tracking analysis (Nanosight NS300, USA) and transmission electron microscope (TECNAI, Japan). The nano-flow cytometry (nanoFCM) of exosome was conducted as previously described [28]. Briefly, the solution of exosomes (5–10 μL) was first diluted with ultrapure water, and then diluted into different concentration. The Cytoflex flow cytometer (Beckman, USA) was employed to determine the most appropriate dilution concentration. Next, the sample (50 μL) was incubated with antibodies (0.25 μL) for 15 min at room temperature to detect the expression level.

The exosomes derived from liver, pancreas or fat tissue were isolated as previous study reported [29]. Firstly, the fresh tissues were dissected and rinsed with ice-cold PBS buffer for three times. Then the tissues were cut into small pieces (2 mm × 2 mm × 2 mm) gently and incubated with collagenase I for 30 min at 37 °C. Filtration and low force centrifugation (300 g, 10 min, once; 3000 g, 20 min, once, 4 °C) were used to remove cells and debris. The resulted supernatant was ultracentrifuged at 100,000 g for 12 h at 4 °C to collect the exosomes.

2.6. Flow cytometry

The cells in the periodontal ligament were collected by enzyme digestion method. The cells were stained with the FITC-CD90 antibody at 37 °C, 15 min, then stained with propidium iodide at 4 °C, 15 min. PDLCs cultured in vitro were directly stained with propidium iodide. The samples were detected and analyzed by flow cytometry (Beckman Coulter, USA). Flowjo V10 is used for data analysis and graph illustration.

2.7. Western blot

Periodontal tissues or PDLCs protein are extracted using RIPA lysis buffer. The periodontal tissues were freezed-ground with 4 mm–5 mm beads in high-speed low-temperature tissue homogenizer (Servicebio, China). The protein concentration was determined by BCA kit and the loading samples were prepared with the concentration of 1 mg mL^{-1}. After electrophoresis using the Bio-Rad system, the proteins on the gel are transferred to the PVDF membrane. The membrane was blocked with 5 % BSA solution at room temperature (RT) for 30 min and incubated with primary antibody at 4 °C overnight. The excess primary antibody was removed by PBST, and the membrane was incubated with the corresponding HRP-conjugated secondary antibody at RT for 1 h. Finally, protein bands were imaged using a chemiluminescent kit (Millipore, USA) by an imaging system (Tanon 4600, China).

2.8. Transmission electron microscopy and immunogold staining

For exosome characterization, exosome suspension (2 μL) was dropped on a 200-mesh carbon-free formvar copper grid for 10 min. After rinsing with ultrapure water twice, the grid was stained with 2 % phosphotungstic acid for 30 s. The grid was finally rinsed with ultrapure water for three times and dried for TEM observation.

For immunogold staining, exosomes were quickly fixed with glutaraldehyde solution for 10 min and then dripped on copper grid for 10 min. Excess suspension was rinsed by ultrapure water and the grid was blocked with 5 % BSA solution. The grid was first incubated with the primary antibody (ASGPR, CYP2E1, 1:20) for 1 h at RT, and subsequently incubated with 10-nm gold-conjugated secondary antibody for 30 min. Then, the grid was rinsed with ultrapure water and stained with 2 % phosphotungstic acid for 30 s. After rinsing and drying, the grids were observed by TEM (TECNAI Spirit FEI, USA).

2.9. Exosomal proteomic analysis

The collected serum was separated by centrifugation at 4000 rpm for 10 min, and the supernatant was used for further isolation of exosomes as described previously [30]. The isolated exosomes were further purified using the Ultra EV isolation kit and stored in screw-top cryogenic vials at ultra-low temperatures. After rapid freezing in liquid nitrogen, the exosomes samples were transported to Lc-Bio Technologies (Hangzhou, China) for subsequent analysis. Upon receipt of the samples, the protein extraction efficiency was evaluated using SDS-PAGE, and 4D-label-free proteomic analysis by time-of-flight mass spectrometry (Thermo Scientific, USA) was performed. The reproducibility of the quantification results was assessed and evaluated, and the differentially expressed proteins were identified and subjected to functional classification and analysis. Based on the statistical results, enrichment analysis was performed using Fisher's exact test. Bioinformatics analysis, including protein database comparison, KEGG enrichment analysis were performed, and data were visualized using the OmicStudio tools.

2.10. In vivo tracing of exosomes

DiR-labelled or DiI-labelled exosomes were administered into mice via tail vein, mice were sacrificed to perform ex vivo bioluminescence imaging by an Imaging system lumina XRMS (PerkinElmer, USA). The luminescent signal was evaluated using Living image software (Calliper Life Sciences, USA). Adeno-associated virus (AAV) with CD63-conjugated GFP/Luciferase and control vector (AAV-Ctrl) was constructed and purified according to standard protocol. Genechem and Hanbio Biotechnology (Shanghai, China) provided technical support in AAV construction. The liver-affinity serotypes 8 and 9 were selected to construct two fluorescence-labelled viruses that were specifically expressed in liver driven by liver-specific promoter TBG or ApoEHCR-hAAT respectively, primer used in construction was listed in Table S2. AAV9-TBG-CD63-luciferase (AAV-CD63-Luc) virus was injected in situ into the liver of db/db mice at a dose of 1.2×10^{11} v.g./mice. Periodontal ligature was performed 2 weeks after infection. After 3 weeks of infection, D-fluorescein (potassium salt) substrate was injected and imaging was performed in vivo. AAV8-ApoEHCR-hAAT-CD63-GFP (AAV-CD63-GFP) was injected in situ into the liver of db/db mice at a dose of 1.2×10^{11} v.g./mice, the other steps are the same as above. After 3 weeks of infection, the samples were collected to observe signal of interest.

2.11. Adenovirus construction and transfection

Mice ADV-Rab27a-shRNA-GFP (ADV-shRab27a), ADV-scramble-shRNA-GFP (ADV-Ctrl) were ordered from Vector Biolabs (PA, USA). For in vivo experiments, adenoviruses (1×10^{10} pfu) were administered via tail vein. At day 2 after injection, mice were ligatured for preparation of periodontitis model. The mice were sacrificed at day 10.

Liver-targeted AAV8-TBG-Fasn-shRNA-GFP (AAV-shFasn) and control vector AAV8-TBG-shRNA-GFP (AAV-Ctrl) were constructed based on validated sequences [31]. To generate these constructs, the exogenous gene was cloned into viral vector and transfected into AAV-293 cells. The virus particles were then collected from the supernatant, concentrated and purified. The virus titer was determined by PCR quantification after confirmation of successful viral construction by sequencing. For animal experiments, a dose of 5×10^{11} v.g./mouse was administered via the tail vein in db/db mice. After 2 weeks, periodontitis model was prepared by ligature, and the animals were sacrificed to perform the subsequent experiments after 3 weeks.

2.12. Animal experiment

All animal experiments were approved by the Animal Ethics Committee of the third affiliated hospital, Fourth Military Medical University. 8-week-old db/db mice obtained from GemPharmatech (Nanjing, China) were regarded as the type 2 diabetes model used in this study. The dynamic blood glucose was detected by glucose meter using the tail blood. The db/m mice in the same litter served as the control. Experimental periodontitis model was established by ligature as previously reported [32]. Concretely, the mice were kept anesthetized by 1.5 % isoflurane, and the mouth was kept exposed with a spreader. Prepare a 15–20 cm length of the 5-0 sterile silk suture ligature with 2 knots in the center (~2 mm apart from each other). Then place the ligature firmly between the first and second molar. Remove the excessive threads away from the knots. After 7 days, experimental periodontitis model was established with a significant decrease in alveolar ridge height detected by micro-CT.

2.13. Micro-CT

To determine the exact level of bone loss and the location of the alveolar ridge, the maxillary jaws of mouse were extracted and scanned by Quantum GX micro-CT (PerkinElmer, USA). Three dimensional histomorphometric data were reconstructed by Mimics software (Materialise, Belgium). The alveolar bone loss level was determined by recording the distance from the cementum-enamel junction to the alveolar bone crest (CEJ-ABC) in first molar (M1).

2.14. Histological analysis

The maxillary bone and the liver of mouse were extracted and fixed with 4 % paraformaldehyde (PFA) for 48 h. The alveolar bone required decalcification in 17 % EDTA (pH = 7.4) for 14 days. Paraffin embedding was performed after dehydration of the maxillary bone and liver. 8-μm thick cross-sections of the periodontal tissue were prepared for H&E staining and immunohistochemical staining. 10-μm thick sections of the liver were prepared for H&E staining, Sirius red, Oil red O staining and immunohistochemical staining according to the manufacturer's instructions. Images were obtained with an histomorphological analysis workstation (Olympus BX41, Japan).

As for immunohistochemical staining, dewaxing and antigen retrieval of the sections are performed first. After endogenous peroxidase was removed by 30 % H_2O_2, the sections were blocked by the goat serum. The sections were then incubated with primary antibody at 4 °C overnight. After washing with PBS, the sections were incubated with secondary antibody for 1 h at RT. Finally, the IHC staining was finished by DAB substrate kit and was counterstained with hematoxylin. The images were captured under the microscope, and the results were analyzed by Image J (NIH, USA).

2.15. Liquid chromatography-mass spectrometry (LC-MS)

After stimulating H-PDLCs with exosomes for 48 h, we collected the cells and supernatant to analyze the content of fatty acids (37 types) using liquid chromatography-mass spectrometry, as shown in Table S3. Metabolites were first extracted from the samples by adding isopropanol:acetonitrilen (1:1, 0.3 mL) and shaking for 1 h. The samples were then centrifuged at 12,000 g for 10 min (4 °C), and the supernatant (95 μL) was mixed with the internal standard (FFA19:0, 5 μL). The solution was transferred to a sample vial for mass spectrometry analysis. Chromatographic separation was performed using an ultra-high performance liquid chromatography system (Waters Corporation, USA), and mass spectrometry analysis was performed using a quadrupole mass spectrometry system (Waters Corporation, USA). The data were quantified using the TargetLynx software.

2.16. Statistical analysis

All experiments in this study were repeated at least three times, and the data were presented as mean ± SD. Statistical analysis was performed by one-way analysis of variance (ANOVA) and Student's *t*-test with SPSS 19.0 (IBM, USA). Tukey or Dunnett's T3 test was used for multiple post hoc comparisons to determine the significance between the groups after one-way ANOVA. The difference between groups was donated statistically significant for $*p < 0.05$, very significant for $**p < 0.01$, and the most significant for $***p < 0.001$. The statistical chart is generated by GraphPad Prism 8.0 (GraphPad Software, USA).

3. Results

3.1. T2DM contributes to pyroptosis in PDLCs and exacerbates alveolar bone loss in periodontitis

T2DM significantly increases the severity of periodontitis with heightened levels of bone destruction and attachment loss. We constructed an experimental periodontitis animal model in db/db mice by thread ligation to investigate the pathogenesis of diabetic periodontitis as previously reported [32] (Figs. S1A–B). At Day 7 after ligation, 3D reconstruction images of micro-CT showed ligation successfully resulted in alveolar bone resorption, and H&E staining showed obvious decrease in the height of the alveolar crest (Fig. 1A). Moreover, there were no serious periodontal lesions in untreated db/db mice, but the alveolar bone loss caused by ligation in db/db mice were more deteriorated than that in db/m mice (Fig. 1A). The distance of cementum-enamel junction to alveolar bone crest (CEJ-ABC) was quantified as an index to identify the degree of alveolar bone resorption. Consistent with the micro-CT analysis, the CEJ-ABC in db/db + Lig mice is significantly higher than that in db/m + Lig mice (Fig. 1B). Notably, osteogenic maker of osteocalcin (OCN) showed the decreased expression in periodontal tissues due to ligation, with the db/db + Lig group displaying the lowest OCN level (Fig. 1A, lower panel and Fig. 1C). These results suggested that we have successfully constructed a diabetic periodontitis model with a more severe degree of alveolar bone loss consistent with clinical symptoms.

Furthermore, the detailed observations of cell fate and status in periodontal tissue were conducted. High-mobility group box 1 (HMGB1) is a highly conserved nuclear protein that leaks into the extranuclear space when cells undergo pyroptosis. It was found from immunohistochemical staining that the release of HMGB1 from the nucleus to the extracellular space in db/db + Lig group was significantly elevated (Fig. 1D). Western blot also confirmed the activation of NLRP3 inflammasome and cleavage of gasdermin D (GSDMD) in periodontal tissue of db/db + Lig mice (Fig. 1E), demonstrating the existence of cell
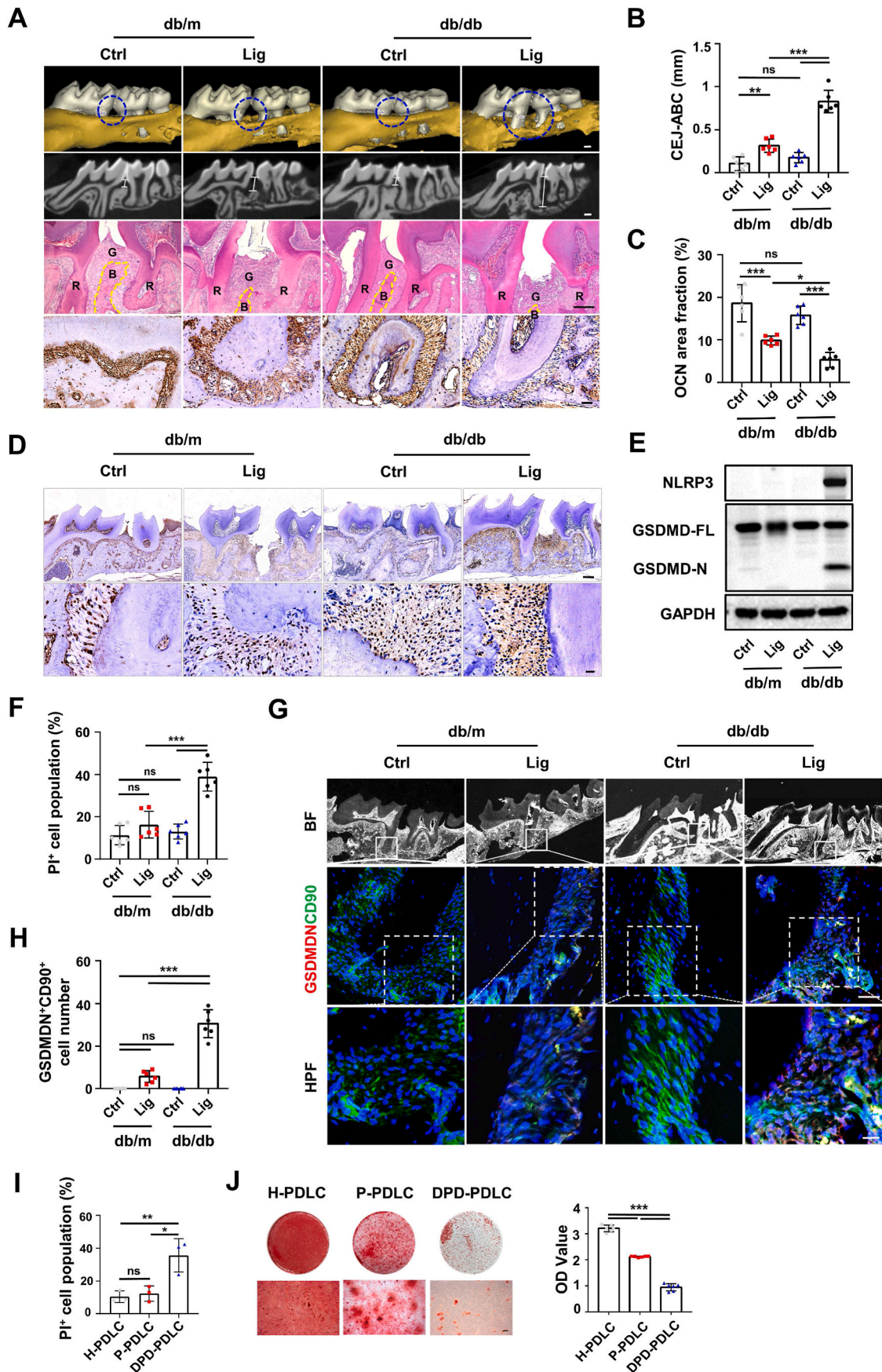
(caption on next page)

Fig. 1. T2DM contributes to pyroptosis in PDLCs and exacerbates alveolar bone loss in periodontitis. (A) The alveolar bone loss of periodontitis in db/db mice was determined by micro-CT and H&E staining. Scale bars, 200 μm. The osteogenic capability was measured by the OCN staining. Scale bars, 50 μm. Ctrl donated untreated group, Lig donated the periodontitis group induced by thread ligature. G: gingiva; B: bone; R: root. **(B)** Quantitative analysis of the distance from cementum-enamel junction to alveolar bone crest (CEJ-ABC) in the micro-CT (n = 6). **(C)** Quantitative analysis of the OCN area fraction in Fig. 1A (n = 6). **(D)** Immunohistochemical staining of HMGB1 expression in the periodontal tissue. Scale bars, 200 μm in low magnification images (top) and 20 μm in high magnification images (bottom). **(E)** Western blot of the NLRP3 and GSDMD expression in the periodontal ligament of different groups. **(F)** The PI-positive ratio of CD90$^+$ PDLCs in periodontal ligament was analyzed by flow cytometry (n = 6). **(G and H)** Representative fluorescence images and quantitative analysis of pyroptotic cells (GSDMDN$^+$CD90$^+$ cells) in periodontal ligament (n = 6). Scale bars, 50 μm in low magnification images (middle) and 20 μm in high magnification images (bottom). **(I–J)** The PI-positive ratio and osteogenic ability of PDLCs isolated from periodontal ligament of healthy individuals (H-PDLC), non-diabetic periodontitis (P-PDLC) and diabetic periodontitis patients (DPD-PDLC) were analyzed by flow cytometry and Alizarin red staining. Scale bars, 200 μm. All results are representative data as mean ± SD. ns, not significant; *$p < 0.05$, **$p < 0.01$, ***$p < 0.001$ by one-way ANOVA.

pyroptosis in periodontal tissue. Periodontal ligament cells (PDLCs), the main cell type of periodontal tissue with the mesenchymal-like property, which are important for the maintenance of the periodontal tissue homeostasis, especially alveolar bone tissue [33]. The occurrence of higher PI-positive rate of CD90$^+$ PDLCs in db/db + Lig mice was confirmed by flow cytometry (Fig. 1F). The N-terminal of GSDMD (GSDMD-N) after cleavage is responsible for the formation of pores in the cell membrane that caused pyroptosis [34]. The co-localization of CD90 and GSDMD-N in periodontal ligament clearly indicated the pyroptosis of PDLCs and more pyroptotic cells were detected in the periodontium of db/db + Lig mice (Fig. 1G and H). Therefore, we speculated that the pyroptosis of PDLCs may be an important reason for the decline of osteogenic ability and aggravation of alveolar bone loss in diabetic periodontitis. In addition, it is widely recognized that hyperglycaemia plays a crucial role in the development of diabetic secondary tissue lesions [35]. However, no significant difference was noticed on blood glucose level between db/db + Lig mice and db/db-Ctrl mice, as well as the db/m + Lig and db/m-Ctrl mice, demonstrating the operation of ligation had no additional effects on the experiment (Fig. S1C).

PDLCs from healthy individuals, non-diabetic periodontitis and diabetic periodontitis patients were isolated for in vitro culture to verify their cell viability and osteogenic ability. The isolated cells were identified as periodontal ligament cells, which is positive for mesenchymal cell markers CD73, CD90 and CD105, and negative for hematopoietic markers CD19, CD34 and CD45 (Fig. S1D). Flow cytometry showed the higher PI-positive ratio in the PDLCs derived from diabetic periodontitis patients compared with other groups (Fig. 1I). Undoubtedly, PDLCs from diabetic periodontitis patients exhibited the worst osteogenic differentiation ability in vitro as shown by the lowest mineralized nodule formation compared with the other groups (Fig. 1J).

Altogether, we concluded that PDLCs pyroptosis in diabetes periodontitis contributed to the decline of osteogenic ability and the deterioration of the alveolar bone loss.

3.2. Circulating exosomes in T2DM induce PDLCs pyroptosis to exacerbate alveolar bone loss in vivo

The elevated circulating exosomes in T2DM are tightly involved in the pathogenesis of diabetic complications by regulating carbohydrate and lipid metabolism [36,37]. Consistent with the previous studies, circulating exosomes level increased significantly in diabetes, while the ligation had no effect on circulating exosomes levels (Fig. 2A). To determine whether elevated exosomes are associated with alveolar bone loss in T2DM, circulating exosome level was inhibited by GW4869, a recognized EVs secretion inhibitor which successfully utilized in vivo [38]. The results showed that GW4869 significantly reduced the level of circulating exosomes in db/db + Lig mice (Fig. 2A), and the followed changes of periodontal lesion were detected (Fig. 2B). Surprisingly, db/db + Lig mice treated with GW4869 resulted in a significant upregulation of bone mass and osteogenic ability evidenced by the CEJ-ABC and OCN expression (Fig. 2C–E). Additionally, the inflammatory HMGB1 staining and TUNEL staining displayed the obvious reduction of pyroptotic cells in periodontal tissue after applying GW4869 in db/db + Lig mice (Figs. S2A–B). The fluorescence co-localization analysis

showed a decreased GSDMD-N level in CD90$^+$ PDLCs after administration of GW4869 (Fig. 2F and G). Flow cytometry analysis emphasized the fluorescent results that the inhibition of circulating exosomes by GW4869 indeed decreased the occurrence of PI-positive PDLCs (Fig. 2H). Western blot also confirmed the reduction of the NLRP3 and GSDMD-N level in periodontal ligament (Fig. S2C). Taken together, these findings suggested that circulating exosomes in diabetes reduced osteogenic capacity by inducing pyroptosis of PDLCs and ultimately increased bone resorption.

3.3. Circulating diabetic exosomes aggravate alveolar bone loss in non-diabetic periodontitis mice

To further confirm the role of circulating exosomes in alveolar bone loss, non-diabetic db/m mice with periodontitis were injected with diabetic circulating exosomes via tail vein to observe the distribution of exosomes and periodontal changes (Fig. 2I). At first, in vivo tracing experiment showed that exosomes were mainly found in alveolar bone over time when entry into circulation, in addition to the routine occurrence in liver for metabolism (Fig. 2J and Figs. S2D–E). Visualization of exosomes in the CD90$^+$ PDLCs by fluorescence staining validated that diabetic circulating exosomes targeted periodontal tissue to regulate PDLCs function in periodontitis (Fig. 2K). In contrast, there was no noticeable enrichment of exosomes in the alveolar bone region of unligated db/m mice (Figs. S2F–H), further consolidating above findings.

Next, the impact of increased diabetic circulating exosomes on alveolar bone formation was explored after accumulation in the periodontal tissue. Micro-CT, H&E and immunohistochemistry staining showed that db/m + Lig mice receiving diabetic exosomes exhibited reduced alveolar ridge height and osteogenic ability (Fig. 2L-N). Leakage of HMGB1 from nucleus to the extracellular space also occurred in periodontal tissue when injected with diabetic exosomes (Fig. S2I). GSDMD-N and PI staining revealed the increased pyroptosis of CD90$^+$ PDLCs (Fig. 2O and P). Likewise, Western blot and TUNEL staining of periodontal tissue indicated that the injection of diabetic circulating exosomes markedly elevated the pyroptosis of PDLCs, leading to increased alveolar bone loss (Figs. S2J–K).

Moreover, the effect of diabetic circulating exosomes on PDLCs was specifically verified in vitro. TNF-α stimulation of PDLCs was used to mimic inflammatory environment of periodontitis [39]. On this basis, circulating diabetic exosomes were added to simulate periodontitis cells in diabetic environment. Exosomes were internalized by PDLCs in time-dependent manner (Figs. S2L-M), indicating the active uptake by cells. Treatment of diabetic exosomes further aggravated the TNF-α-induced decline in osteogenic ability of PDLCs evidenced by the reduced mineralization nodule formation (Fig. 2Q). Fluorescence staining verified that the PDLCs receiving exosomes suffered an uncontrolled spillover of HMGB1 from the nucleus (Fig. S2N). Flow cytometry, TUNEL staining and CCK8 confirmed that pyroptosis in PDLCs arose when exposed to diabetic circulating exosomes (Fig. 2R and S2O-P). Western blot of the extracted cellular proteins exhibited high levels of NLRP3 and GSDMD cleavage in the exosome-treated PDLCs (Fig. 2S).
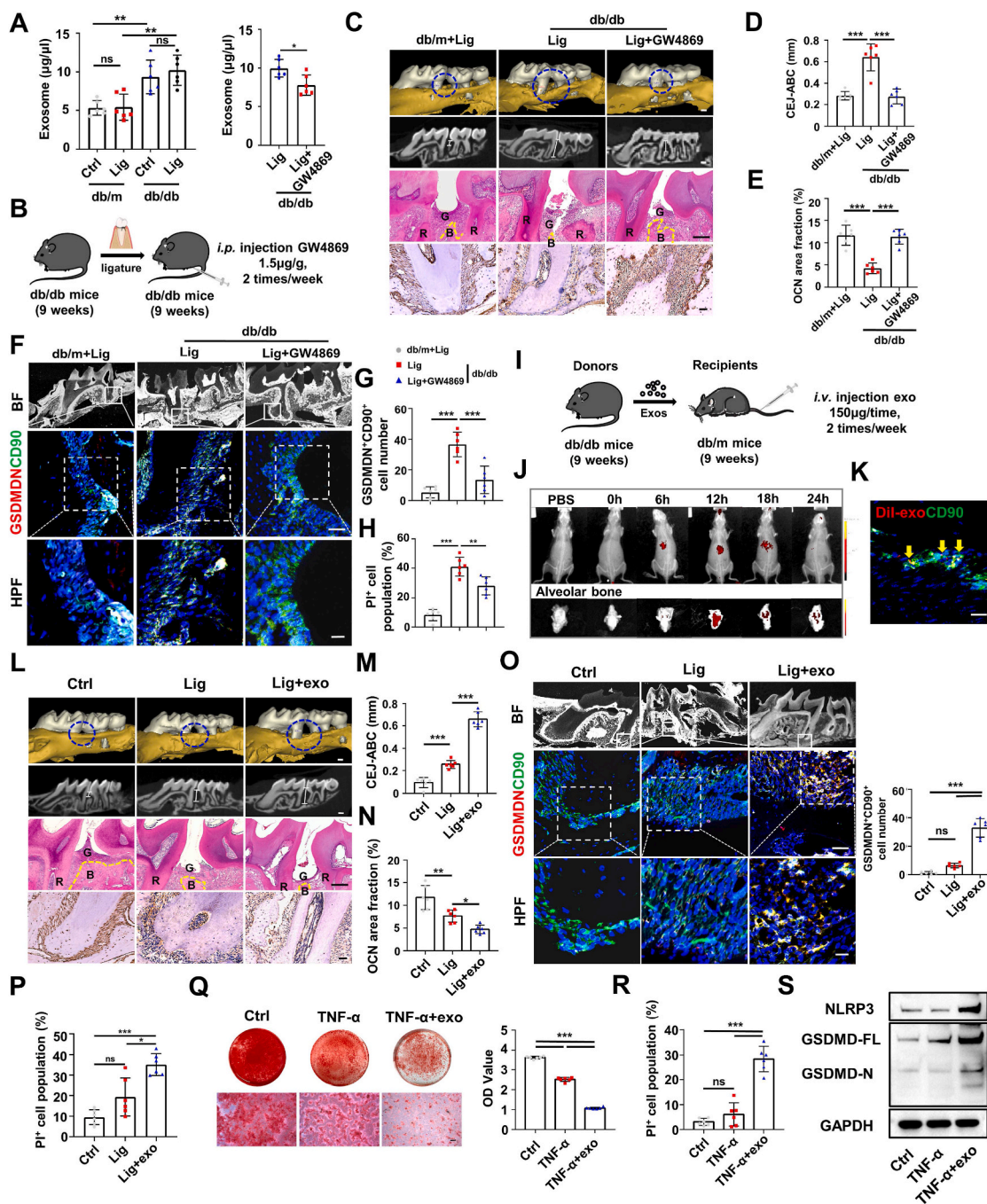
Fig. 2. Circulating exosomes in T2DM induce pyroptosis of PDLCs to exacerbate alveolar bone loss in periodontitis. (A) Detection of circulating exosome levels in different groups (n = 6). **(B)** Experimental scheme shows periodontitis model with exosome inhibition in db/db mice. **(C)** The alveolar bone loss of periodontitis in db/db mice with exosome inhibition was determined by micro-CT, H&E staining. Scale bars, 200 μm. The assessment of osteogenic capability was performed through immunohistochemistry staining of OCN. Scale bars, 50 μm. G: gingiva; B: bone; R: root. **(D)** Quantitative analysis of the distance of CEJ-ABC in the micro-CT (n = 6). **(E)** Quantitative analysis of the OCN area fraction in Fig. 2C (n = 6). **(F and G)** Representative fluorescence images and quantitative analysis of pyroptotic cells (GSDMDN⁺CD90⁺ cells) in periodontal ligament of db/db mice with exosomes inhibition (n = 6). Scale bars, 50 μm in low magnification images (top) and 20 μm in high magnification images (bottom). **(H)** The PI-positive ratio of CD90⁺ PDLCs in periodontal ligament was analyzed by flow cytometry with exosome inhibition in db/db mice (n = 6). **(I)** Experimental scheme shows periodontitis model in db/m mice supplemented with circulating exosomes from db/db mice. **(J)** The enrichment of exosomes in the periodontal region showed by in vivo imaging. **(K)** DiI-exosomes are internalized by CD90⁺ PDLCs. Scale bars, 20 μm. **(L)** The alveolar bone loss of db/m mice supplemented with circulating diabetic exosomes was determined by micro-CT, H&E staining. Scale bars, 200 μm. The assessment of osteogenic capability was performed through immunohistochemistry staining of OCN. Scale bars, 50 μm. **(M and N)** Quantitative analysis of the CEJ-ABC and OCN area fraction in Fig. 2L (n = 6). **(O)** Representative fluorescence images and quantitative analysis of GSDMDN⁺CD90⁺ cells in periodontal ligament of db/m mice supplemented with circulating diabetic exosomes (n = 6). Scale bars, 50 μm in low magnification images (top) and 20 μm in high magnification images (bottom). **(P)** The proportion of PI-positive cells was measured by flow cytometry (n = 6). **(Q)** Diabetic circulating exosomes impaired the osteogenic capacity of PDLCs. Scale bars, 200 μm. **(R)** Diabetic circulating exosomes induced the PI-positive ratio of PDLCs showed by flow cytometry (n = 6). **(S)** Western blot analysis of NLRP3 and GSDMD in PDLCs treated with diabetic circulating exosomes. All results are representative data as mean ± SD. ns, not significant; *p < 0.05, **p < 0.01, ***p < 0.001 by Student's t-test and one-way ANOVA.

These results indicated that the elevated circulating exosomes in T2DM migrated to and enriched in the alveolar bone of periodontitis, leading to the pyroptosis of PDLCs and consequent alveolar bone loss.

3.4. Exosomes secreted by liver migrate to periodontal tissue in T2DM

To elucidate the mechanism underlying the detrimental effect of diabetic exosomes on alveolar bone loss in periodontitis, the contents and distribution of exosomes should be dissected in detail. The circulating exosomes of db/db mice and db/m mice were purified to perform 4D label-free proteomic sequencing analysis. At first, the characterization displayed the typical bilayer membrane structure and standard particle size range (40–150 nm) (Figs. S3A–C). In addition, Western blot revealed the positive markers CD63, TSG101 and Alix, rather than GM130 and Calnexin in exosomes (Fig. S3D).

Bioinformatics analysis and comparison with protein database revealed a higher enrichment of proteins in the metabolic pathway, with the most significant differential protein enrichment found in the fatty acid metabolism and biosynthesis pathways (Fig. S3E). As the dysregulation of lipid metabolism often existed in individuals with T2DM [40], it is reasonable to assume that these proteins related to lipid metabolism might be involved in exosomes function. The main differentially expressed proteins between the two groups of exosomes were identified by cluster analysis (Fig. 3A), among which Fasn was one of the most obvious differences proteins (Fig. 3B). Fasn (fatty acid synthase) is primarily expressed in the liver, adipose tissue and lactating mammary glands, where it plays a crucial role in de novo fatty acid biosynthesis [41]. Therefore, circulating exosomes may mainly originate from these tissues and enter the circulation.

To clarify the source of circulating exosomes under T2DM impairment, exosomes from liver, pancreas, and fat tissue of db/db mice were extracted, characterized and injected into db/m mice to observe the effect on alveolar bone loss (Figs. S3F–H). Micro-CT found that exosomes derived from the liver resulted in the most severe bone resorption in db/m + Lig mice (Fig. 3C and D). Furthermore, H&E staining of liver tissue from db/db mice showed vacuolar degeneration, and positive Oil Red O staining indicated liver steatosis (Fig. 3E). Sirius red staining showed no signs of fibrosis (Fig. 3E). Additionally, the expression of Fasn in the liver of db/db mice was found to be upregulated compared to liver of db/m mice (Fig. 3E), suggesting the abnormal fatty acid metabolism in liver during diabetes. Since the liver is the primary metabolic center of the body and the characteristic lesion site of diabetes, we suspected that exosomes generated by the liver contained with Fasn were secreted into the circulation to participate in the regulation of physiological homeostasis.

To determine whether the circulating exosomes were derived from liver, we employed specific liver cell markers to identify them. NanoFCM found that 31.02% of circulating exosomes expressed asialoglycoprotein receptor (ASGPR) which is predominantly expressed on the surface of liver cells [42], suggesting that almost one-third of circulating exosomes may originate from the liver in diabetic host (Fig. 3F). Immunogold electron microscopy revealed the presence of both ASGPR and CYP2E1 on exosomes surface (Fig. 3G). The increased expression of Albumin and ASGPR on exosomes of db/db mice was detected by Western blot (Fig. 3H), indicating an elevated secretion level of exosomes derived from the liver in circulation. The above experiments preliminarily demonstrated that a majority of circulating exosomes originated from the liver. To further detect the distribution of exosomes from liver in vivo, the labelled liver exosomes were injected into db/m + Lig mice intravenously. The presence of liver-exosomes in CD90+ PDLCs of the periodontal region was noticed (Fig. 3I). Moreover, a hepatocyte-specific virus was constructed by fusing CD63 with luciferase (AAV-CD63-Luc) to label liver exosomes. After injection of the purified virus into db/db + Lig mice, in vivo imaging revealed the strong fluorescence signal accumulated in the liver and the ligatured region of the alveolar bone (Fig. 3J), confirming that liver-derived CD63-positive

exosomes migrated to the alveolar bone region. Furthermore, another liver-targeted AAV-CD63-GFP virus was injected into db/db + Lig mice. After 3 weeks, GFP-labelled liver exosomes were present in periodontal region (Fig. 3K). More evidence was provided by the fluorescence imaging to determine the distribution of exosome from each tissue in periodontal tissue by specific marker ASGPR (liver), Adiponectin (fat tissue) and PDX1 (pancreas). The results indicated that the presence of periodontitis significantly increased the local aggregation of tissue exosomes in the periodontal region, with the most abundant are liver exosomes (Fig. S3I). These in vivo tracing results suggested that liver exosomes could reach inflammation sites in the alveolar bone from the circulation.

Altogether, these data demonstrated that metabolically impaired liver in diabetes promoted the release of Fasn-carrying exosomes, which are recruited to the periodontal region to regulate PDLCs function.

3.5. Specific inhibition of liver exosomes secretion alleviates alveolar bone loss in diabetic periodontitis

To further confirm the functional role of liver exosomes on alveolar bone in diabetic periodontitis, Rab27a was inhibited in liver to reduce the secretion of exosome [43]. ADV-shRab27a-GFP virus (ADV-shRab27a) for knockdown of Rab27a in liver was utilized to effectively reduce liver exosomes secretion previously [44,45]. Intravenously injection of ADV-shRab27a and ADV-shCtrl into db/db + Lig mice showed a high hepatotropism (Fig. 4A). Intriguingly, liver tissue sections revealed a significant increase of Rab27a expression in liver of db/db mice compared to db/m mice (Fig. S4A), whereas injection with the ADV-shRab27a in db/db mice resulted in a significant decrease in Rab27a expression (Fig. 4B and C). Administration of ADV-shRab27a significantly reduced the ASGPR+ population in circulating exosomes (Fig. S4B), and the ASGPR+ liver-exosomes presented in periodontal region in periodontitis were also decreased (Fig. S4C), confirming the successful inhibition of exosomes secreted by liver. Subsequently, inhibition of liver exosomes alleviated alveolar bone loss and partially restored osteogenic capacity in db/db + Lig mice (Fig. 4D–F). The release of HMGB1 was reduced, and the pyroptotic population of CD90+ PDLCs was significantly decreased in periodontium after inhibiting exosomes secretion by ADV-shRab27a (Fig. 4G–I and Fig. S4D). Western blot also proved that ADV-Rab27a relieved the NLRP3 activation and cleavage of GSDMD (Fig. S4E). Furthermore, the db/db + Lig mice with Rab27a inhibition by ADV-Rab27a were reinjected with db/db-liver exosomes intravenously. This group that received db/db-liver exosomes exhibited increased CEJ-ABC and decreased osteogenic ability (Fig. 4D–F). The improved periodontal lesions in shRab27a-treated mice were all vanished by the supplement of exogenous db/db-liver exosomes, accompanied with the elevated level of HMGB1 release and pyroptotic cells in periodontal tissues (Fig. 4G–I and Figs. S4D–F). In addition, db/db-liver exosome also led to the pyroptosis of PDLCs and deteriorated alveolar bone loss in db/m + Lig mice, but db/m-liver exosomes generate no such effect (Figs. S4G–H). These results accurately illustrated that liver exosomes weakened osteogenic capacity and exacerbated bone loss by induction of PDLCs pyroptosis in diabetic periodontitis.

Similarly, the application of purified exosomes from diabetic liver tissue to TNF-α-stimulated PDLCs yielded the same results. As with circulating exosomes, liver-derived exosomes significantly reduced the osteogenic differentiation ability of PDLCs showed by Alizarin red staining (Fig. 4J), and contributed to the occurrence of PDLCs pyroptosis (Fig. 4K-L and Figs. S4I–J).

Altogether, these results illuminated that abnormal liver-derived exosomes mediated pyroptosis of PDLCs in T2DM, resulting in exacerbation of periodontal bone loss.
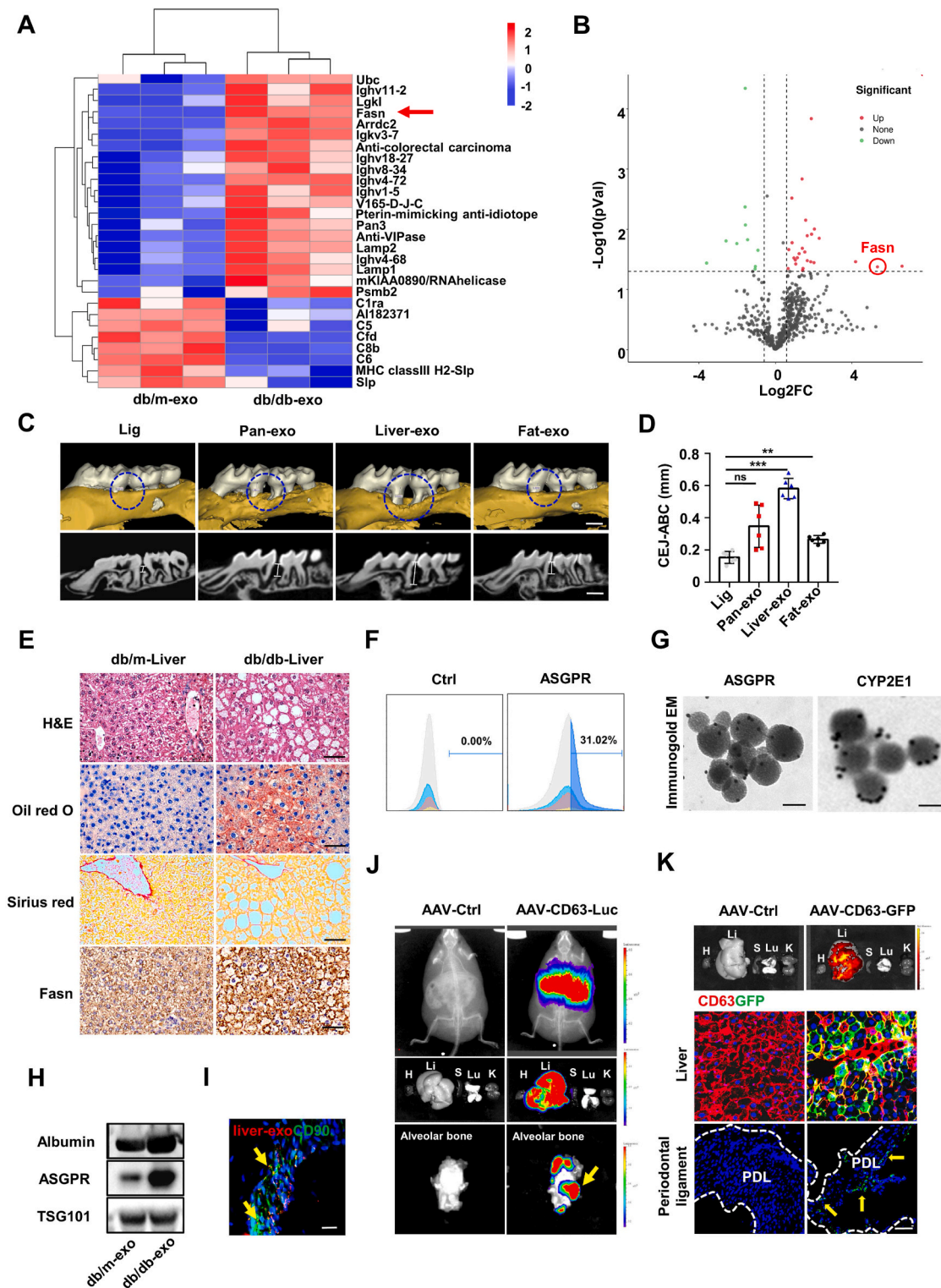
Fig. 3. Exosomes secreted by metabolically impaired liver in T2DM migrate to periodontal tissue. (A) Cluster analysis of differentially expressed proteins (P value < 0.05 and Fold change >1.5) between db/m-exo and db/db-exo, with proteins abundance being Z-score normalized. **(B)** Volcano plots showed the fold change of different proteins. The green and red dots indicate down-regulated and up-regulated proteins, respectively. **(C)** The alveolar bone loss in db/m + Lig mice treated with exosome derived from different tissues was determined by micro-CT. Scale bar, 200 μm. **(D)** Quantitative analysis of the CEJ-ABC in the micro-CT (n = 6). **(E)** Histological evaluation of liver by H&E staining, Oil red O, Sirius red, and Fasn staining. Scale bars, 50 μm. **(F)** The expression of ASGPR on diabetic circulating exosomes analyzed by NanoFCM. **(G)** Immunoelectron microscopy detection of ASGPR and CYP2E1 in diabetic circulating exosomes. Scale bars, 100 nm. **(H)** The expression of ASGPR and Albumin was measured in circulating exosomes. **(I)** DiI-labelled liver-exosomes are internalized by CD90$^+$ PDLCs in periodontal ligament. Scale bars, 20 μm. **(J)** The enrichment level of endogenous liver exosomes in periodontal bone site determined by in vivo imaging. H: heart; Li: liver; S: spleen; Lu: lung; K: kidney. **(K)** Fluorescence images showed the distribution of endogenous liver exosomes in periodontal ligament labelled by AAV-CD63-GFP. H: heart; Li: liver; S: spleen; Lu: lung; K: kidney. Scale bars, 50 μm. All results are representative data as mean ± SD. ns, not significant; **$p < 0.01$, ***$p < 0.001$ by one-way ANOVA. (For interpretation of the references to colour in this figure legend, the reader is referred to the web version of this article.)
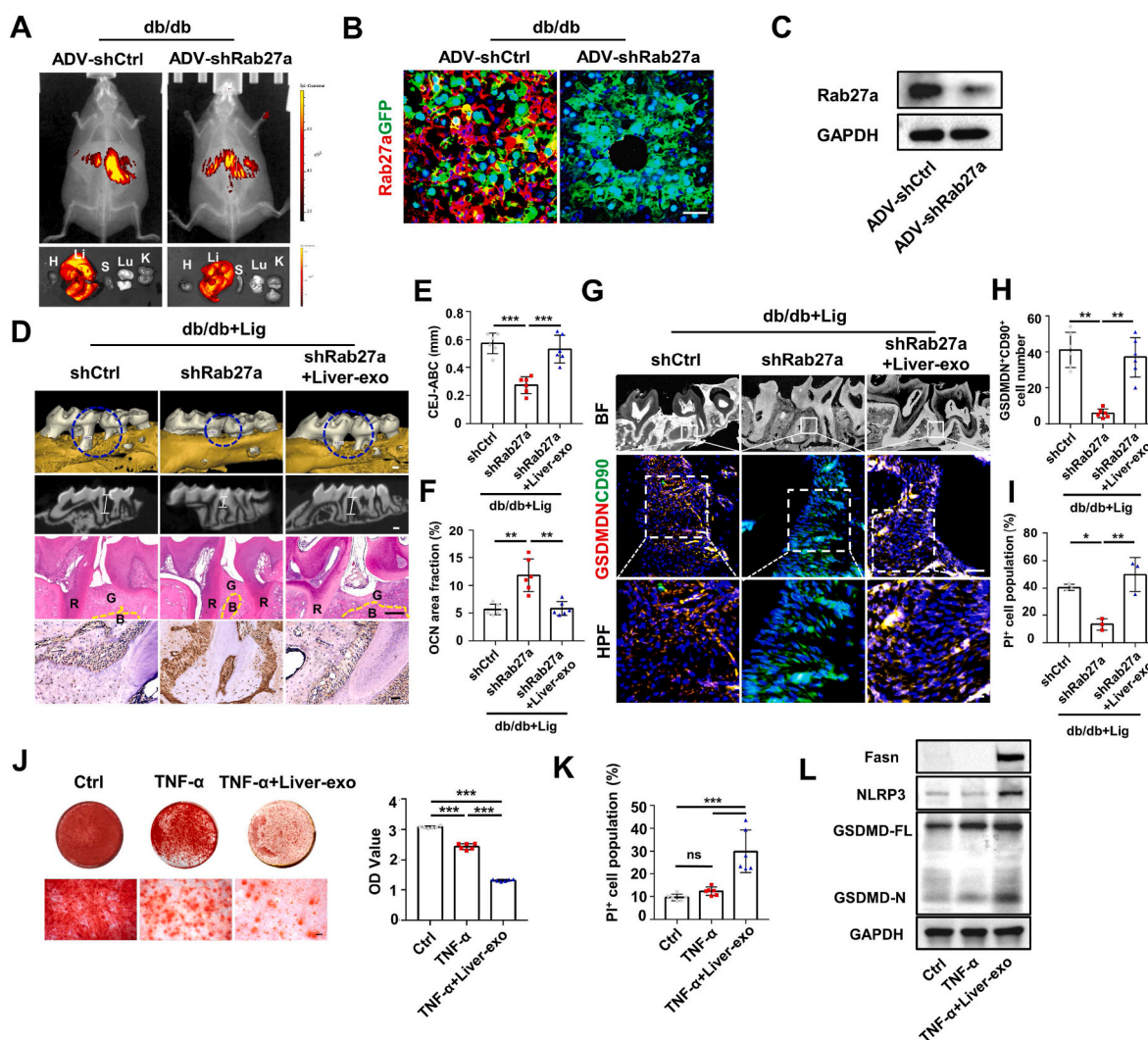
Fig. 4. Inhibition of endogenous liver exosomes ameliorates alveolar bone loss in diabetic periodontitis mice. (A) In vivo imaging showed that the adenovirus (ADV) is highly enriched in the liver. **(B and C)** ADV-shRab27a effectively reduced the expression of Rab27a in liver. Scale bars, 50 μm. **(D)** The alveolar bone loss of diabetic periodontitis mice with knockdown of Rab27a were determined by micro-CT, H&E staining. Scale bars, 200 μm. Osteogenic ability was determined by immunohistochemistry staining of OCN. Scale bars, 50 μm. G: gingiva; B: bone; R: root. **(E and F)** Quantitative analysis of the CEJ-ABC and the OCN area fraction in Fig. 4D (n = 6). **(G and H)** Representative fluorescence images and quantitative analysis of pyroptotic cells (GSDMDN⁺CD90⁺ cells) in periodontal ligament (n = 6). Scale bars, 50 μm in low magnification images (top) and 20 μm in high magnification images (bottom). **(I)** The proportion of PI-positive cells in periodontal ligament measured by flow cytometry (n = 3). **(J)** Exosomes derived from diabetic liver impaired the osteogenic capacity of PDLCs. Scale bars, 200 μm. **(K)** The PI-positive ratio of PDLCs by flow cytometry (n = 6). **(L)** The expression of Fasn, NLRP3 and GSDMD was detected in PDLCs treated with exosomes derived from diabetic liver. All results are representative data as mean ± SD. *$p < 0.05$, **$p < 0.01$, ***$p < 0.001$ by one-way ANOVA.

3.6. Knockdown of Fasn rescues alveolar bone loss and periodontal pyroptosis in vivo

Fasn was screened as the candidate molecule for the pathogenic process by the proteomic analysis. Fluorescent staining revealed an upregulation of Fasn expression in the liver of db/db mice compared with db/m mice (Fig. S5A), consistent with the results in Fig. 3E. Here, Western blot confirmed the presence of Fasn in the exosomes of db/db mice, while Fasn was almost absent in db/m exosomes (Fig. S5B). The expression of Fasn is relatively low in periodontal tissue of db/m + Lig mice, but is high in the periodontal tissue of db/db + Lig mice (Fig. S5, C and E). Inhibition of circulating exosomes by GW4869 reduced Fasn level in periodontal tissues (Fig. S5, C and E). Moreover, administration of diabetic circulating exosomes in db/m + Lig mice elevated Fasn levels in the periodontal tissue (Fig. S5, D and F), suggesting Fasn may be the pathogenic factor carried in exosomes. As expected, the Fasn level was reduced to an almost undetectable level after liver exosome inhibition via ADV-Rab27a (Fig. 5A and Fig. S4E). And liver-exosome re-

supplementation indeed restored abnormally high expression level of Fasn in periodontal tissue of db/db + Lig mice (Fig. 5A and Fig. S4E), confirming that liver exosomes are the main vehicle of Fasn into periodontal tissues.

To know whether enhanced alveolar bone loss is attributed to the abnormal Fasn expression, virus that targets the liver for knockdown of Fasn (AAV-shFasn) was injected into db/db + Lig mice. In vivo imaging revealed effective targeting of AAVs to the liver and reduction of Fasn level in liver (Fig. 5B and Figs. S5G–H). There was also a more obvious decrease of Fasn in the liver exosomes (Fig. 5C). After successful knockdown of Fasn in the liver-secreted exosomes, the Fasn level in periodontal tissue was evidently decreased in db/db + Lig mice (Fig. 5D and Fig. S5I). Consequently, decreased Fasn in periodontal tissue generated a beneficial effect on periodontal lesion with reduced bone resorption and improved osteogenic capacity (Fig. 5E–G). Alleviated HMGB1 release and declined PDLCs pyroptosis preliminarily explained the improvement of periodontal cell function (Fig. 5H–I and Figs. S5I–K). Western blot also showed a decrease in NLRP3 expression
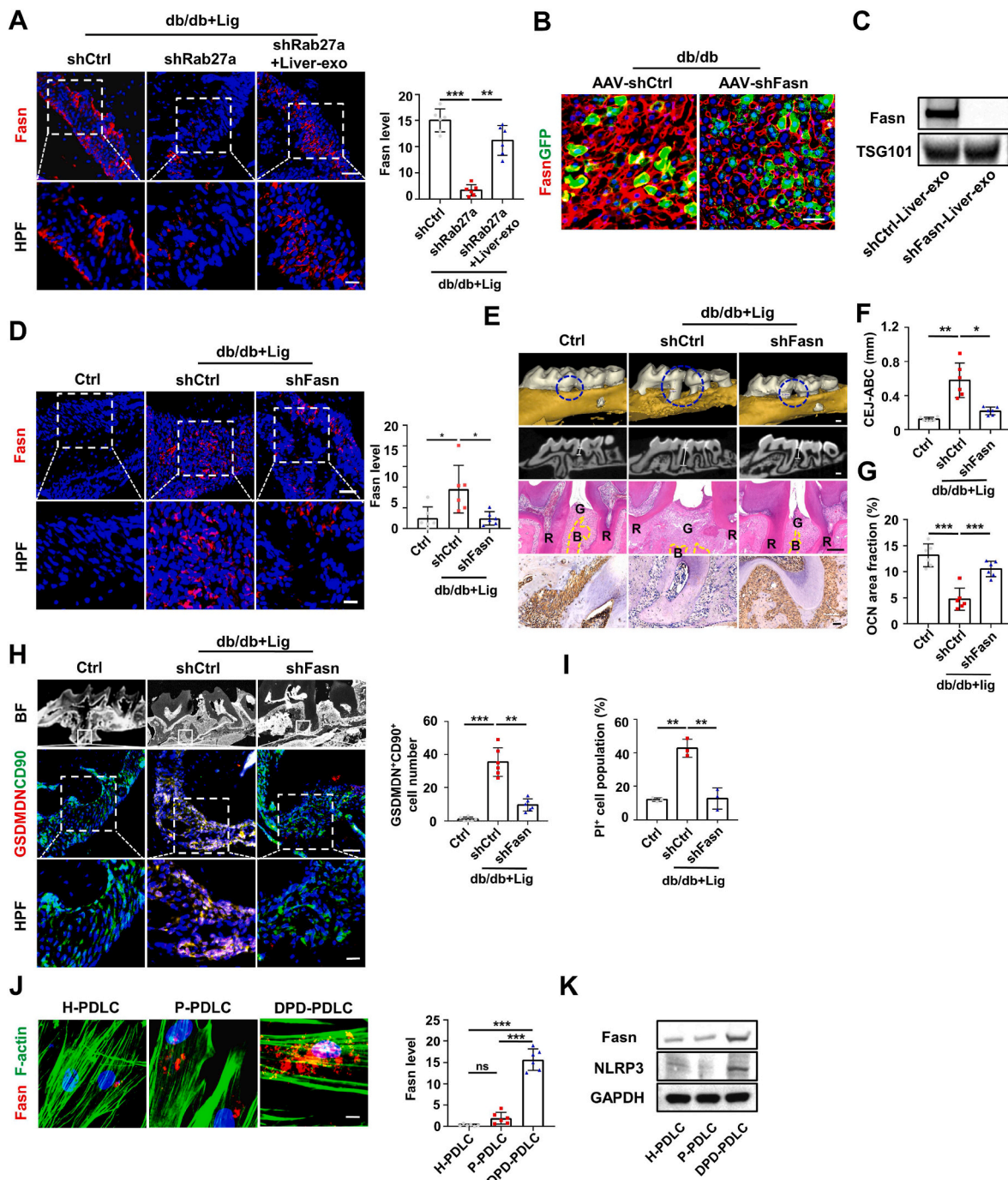
Fig. 5. Specific knockdown of Fasn in liver exosomes effectively reduces pyroptosis and rescues osteogenic ability. **(A)** Representative fluorescence images and quantitative analysis of Fasn level in periodontal ligament after inhibition and re-supplement of liver exosomes (n = 6). Scale bars, 50 μm in low magnification images (top) and 20 μm in high magnification images (bottom). **(B)** AAV-shFasn effectively reduced the expression of Fasn in liver by fluorescence image. Scale bars, 50 μm. **(C)** Western blot showed that AAV-shFasn effectively declined Fasn level in liver exosomes. **(D)** The Fasn level in periodontal ligament of diabetic peri-odontitis mice after administration of AAV-shFasn (n = 6). Scale bars, 50 μm in low magnification images (top) and 20 μm in high magnification images (bottom). **(E)** The alveolar bone loss of diabetic periodontitis mice with Fasn knockdown in liver was determined by micro-CT, H&E staining. Scale bars, 200 μm. Osteogenic ability was determined by immunohistochemistry staining of OCN. Scale bars, 50 μm. G: gingiva; B: bone; R: root. **(F and G)** Quantitative analysis of the CEJ-ABC and OCN area fraction in Fig. 5E (n = 6). **(H)** Representative fluorescence images and quantitative analysis of pyroptotic cells (GSDMDN$^+$CD90$^+$ cells) in periodontal ligament (n = 6). Scale bars, 50 μm in low magnification images (top) and 20 μm in high magnification images (bottom). **(I)** The proportion of PI-positive cells in periodontal ligament was measured by flow cytometry (n = 3). **(J)** The Fasn expression of PDLCs from healthy individuals (H-PDLC), non-diabetic periodontitis (P-PDLC) and diabetic periodontitis patients (DPD-PDLC). Scale bars, 10 μm. **(K)** The Fasn and NLRP3 expression in PDLCs from patients confirmed by Western blot. All results are representative data as mean ± SD. ns, not significant; *$p < 0.05$, **$p < 0.01$, ***$p < 0.001$ by one-way ANOVA.

and inhibition of GSDMD cleavage (Fig. S5I).

Additionally, it is very exciting that high level of Fasn was found in PDLCs derived from diabetic periodontitis patients, which is not excessively expressed in PDLCs from the other sources (Fig. 5J and K). Meanwhile, PDLCs derived from diabetic periodontitis patients also revealed a higher incidence of activated NLRP3 inflammasome, suggesting the occurrence of pyroptosis in vivo (Fig. 5K). In vitro, both circulating exosomes and liver-exosomes from db/db mice resulted in the upregulation of Fasn in PDLCs (Fig. 4L and Figs. S5L-M), confirming Fasn carried in exosomes secreted by liver is a key molecule that leads to periodontal cell pyroptosis.

3.7. Fasn carried in exosomes induces pyroptosis in PDLCs by ectopic synthesis of fatty acid

To elucidate the detailed mechanism of pyroptosis induced by Fasn to trigger osteogenic dysfunction of PDLCs, C75 was used to inhibit the high activity of Fasn in PDLCs. Alizarin red staining showed that C75 effectively reversed the loss of osteogenic differentiation ability of

PDLCs caused by diabetic liver-exosomes (Fig. 6A). The occurrence of cell pyroptosis caused by liver-exosome was substantially ameliorated with C75 (Fig. 6B–E). The pyroptosis of PDLCs caused by diabetic circulating exosomes was also mitigated by the application of C75 (Figs. S6A–D). These findings provide the evidence that blockage of Fasn activity can directly alleviate pyroptosis and restore PDLCs function.

Subsequently, the downstream pathway by which Fasn triggered pyroptosis was further investigated. Since C75 effectively restrained the synthesis of fatty acids by Fasn [31], fatty acids produced by PDLCs after the treatment of circulating exosomes or liver-exosomes from db/db mice were collected for detection by liquid chromatography-mass spectrometry analysis. A total of 37 types of fatty acids were detected, with palmitic acid, stearic acid and oleic acid being the top three in terms of abundance (Fig. 6F, Table S3). The results indicated that treatment of diabetic circulating exosomes or liver-exosomes significantly enhanced the production of fatty acids in PDLCs, which was reversed by application of C75. Among them, palmitic acid (PA) accounted for the highest proportion, with the most significant difference compared to the control group (Fig. 6F and Fig. S6E). PA is the
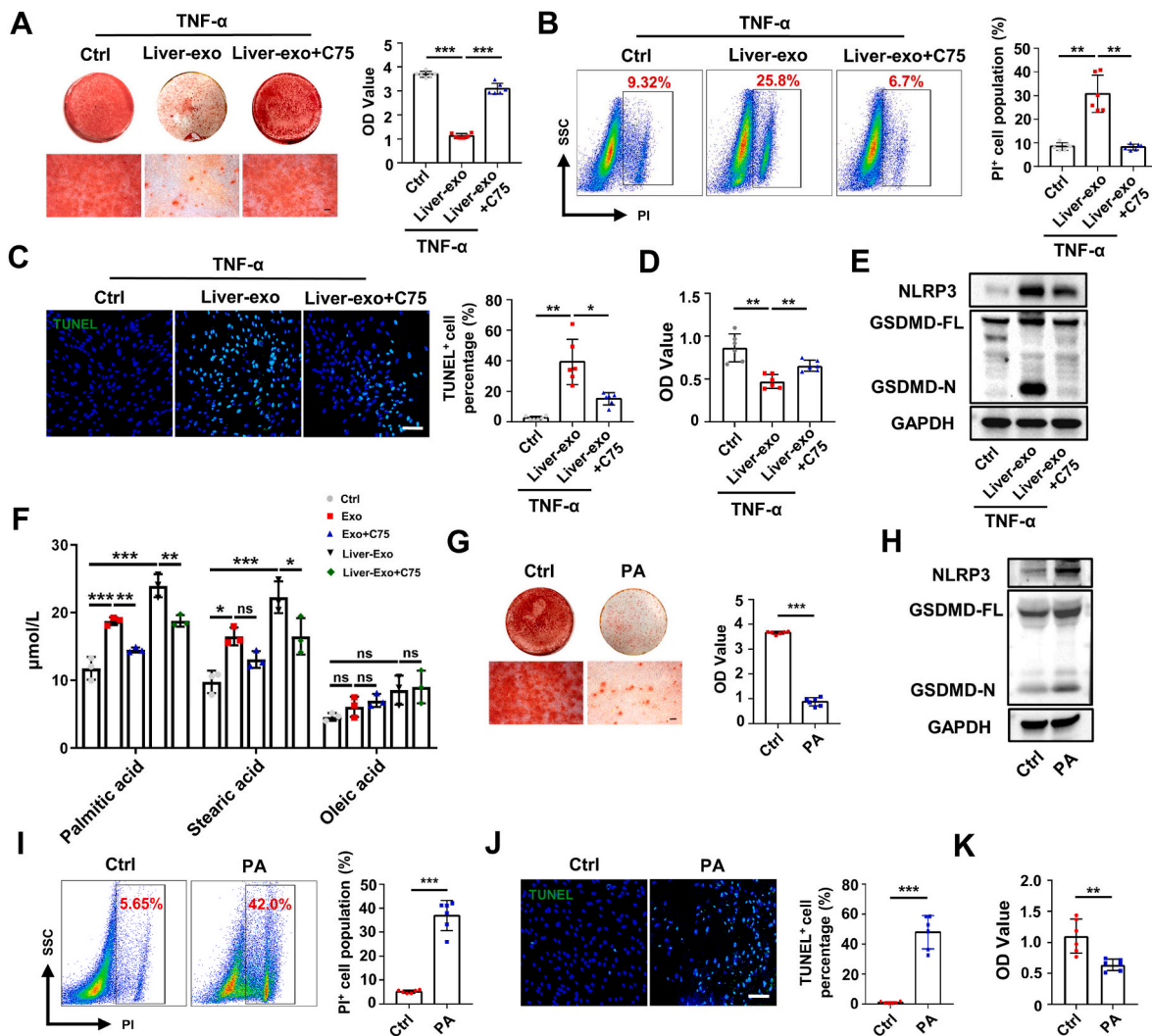
Fig. 6. Excessive fatty acid synthesis induced by Fasn results in pyroptosis and dysfunction of PDLCs. (A) The osteogenic ability of PDLCs was rescued with Fasn inhibition by C75. Scale bars, 200 μm. **(B and C)** Flow cytometry and TUNEL staining showed that C75 mitigated the PI-positive ratio of PDLCs induced by liver-exosomes (n = 6). Scale bars, 100 μm. **(D)** The cell viability of PDLCs detected by CCK8 assay (n = 6). **(E)** The expression of NLRP3 and GSDMD was detected in liver-exosome-treated PDLCs after C75 application. **(F)** Analysis of fatty acid production in PDLCs after exosomes treatment with or without C75 application by liquid chromatography-mass spectrometry (n = 3). **(G)** The osteogenic ability of PDLCs was impaired by palmitic acid. Scale bars, 200 μm. **(H)** The expression of NLRP3 and GSDMD was detected in PDLCs treated with palmitic acid. **(I–J)** The PI staining and TUNEL staining of PDLCs after treatment of palmitic acid (n = 6). Scale bars, 100 μm. **(K)** The cell viability of PDLCs after treatment of palmitic acid by CCK8 assay (n = 6). All results are representative data as mean ± SD. ns, not significant; *$p <$ 0.05, **$p <$ 0.01, ***$p <$ 0.001 by one-way ANOVA and Student's *t*-test.

main pathogenic substance inducing pyroptosis in various cell types [46, 47], and this process involves the NLRP3 inflammasome [48]. When Fasn activity was inhibited by C75, PA was the most sensitive product no matter which exosome was treated (Fig. 6F). Consequently, the effect of PA on PDLCs was examined in vitro, and the results displayed that PA reduced the osteogenic differentiation capacity of PDLCs (Fig. 6G). Mechanistically, PA induced pyroptosis in PDLCs by activation of the NLRP3 inflammasome and GSDMD cleavage (Fig. 6H–K). However, stearic acid (SA), which showed increased expression after exosomes treatment, did not induce PDLCs dysfunction and pyroptosis (Figs. S6F–J).

Therefore, these data indicated that Fasn caused pyroptosis through the ectopic synthesis of fatty acids in PDLCs.

In summary, our finding reveals that excessive Fasn migrated to the periodontal lesion through secreted exosomes from impaired liver, resulting in the ectopic synthesis of fatty acids represented by palmitic acid in PDLCs. The abnormal presence of fatty acids activated NLRP3 inflammasome, initiated the cleavage of GSDMD and induced pyroptosis of PDLCs, which ultimately generated the severe and refractory clinical symptoms displayed as worsening of periodontal osteogenic ability and deterioration of alveolar bone loss (Fig. 7). These findings shed light on the role of extracellular vesicles in the regulation of bone homeostasis and have implications for novel therapeutic strategies focused on fatty acid metabolism in diabetic bone disorders.

4. Discussion

Existing retrospective clinical analysis suggested that diabetic patients have more rapidly progressing periodontitis than non-diabetic patients, which often was presented as incomplete or immature bone formation [49]. Diabetic patients frequently encounter challenges in bone regeneration, even after adequate blood glucose control and periodontal treatment [50]. Extracellular vesicles (EVs) are currently a special kind of natural bioactive nanoparticles in the body, acting as both biological mediators and potential drug delivery systems [14,18]. Inspired by this, we established an undescribed mode mediated by EVs to elucidate the specific correlation between periodontitis and diabetes. Compared with previous studies, our work found that exosomes derived from liver served as modulators to trigger the pyroptosis and osteogenic dysfunction of PDLCs, thus revealing a communication pattern based on the "liver-bone" axis under metabolic disorders. Emerging studies contributed to the understanding of the crucial liver-bone axis in maintaining systemic metabolic homeostasis [51,52]. Small EVs from periodontitis patients were found to mediate the insulin resistance in T2DM [53]. Since liver is an essential metabolic organ, the disturbance under diabetes will bring the inevitable effect on the healing process occurring in distant region by EVs, which shed light on other diabetic peripheral complications such as diabetic foot ulcers and diabetic skin infections.

Diabetes is a systemic metabolic disorder that has been identified as a potential risk factor for tissue healing. As the main effector cells of bone regeneration, PDLCs was found to execute pyroptosis in diabetic periodontitis, which exactly explained the severe osteogenic deficiency and exacerbated bone loss. Pyroptosis is a newly emerged type of programmed cell death that often occurs in inflammatory tissue damage. Cell disintegration will produce immunogenic inflammation and further aggravate tissue destruction. Previous researches have reported that pyroptosis mediated the release of DAMPs, contributing to the inflammatory response in chronic disease such as atherosclerosis, diabetes and neurodegeneration [54]. This is the first time to introduce pyroptosis in the pathogenesis of diabetic periodontitis. Although the existence of other cell death forms or dysfunction of other cells cannot be ruled out, this study highlighted the crucial role of PDLCs during alveolar bone formation.

Fasn is a multifunctional enzyme contributing to the synthesis of endogenous fatty acids in lipid metabolism, which is highly expressed in liver cells, but little in periodontal cells. The liver damage associated with diabetes led to the high level of Fasn, which transfer to where it
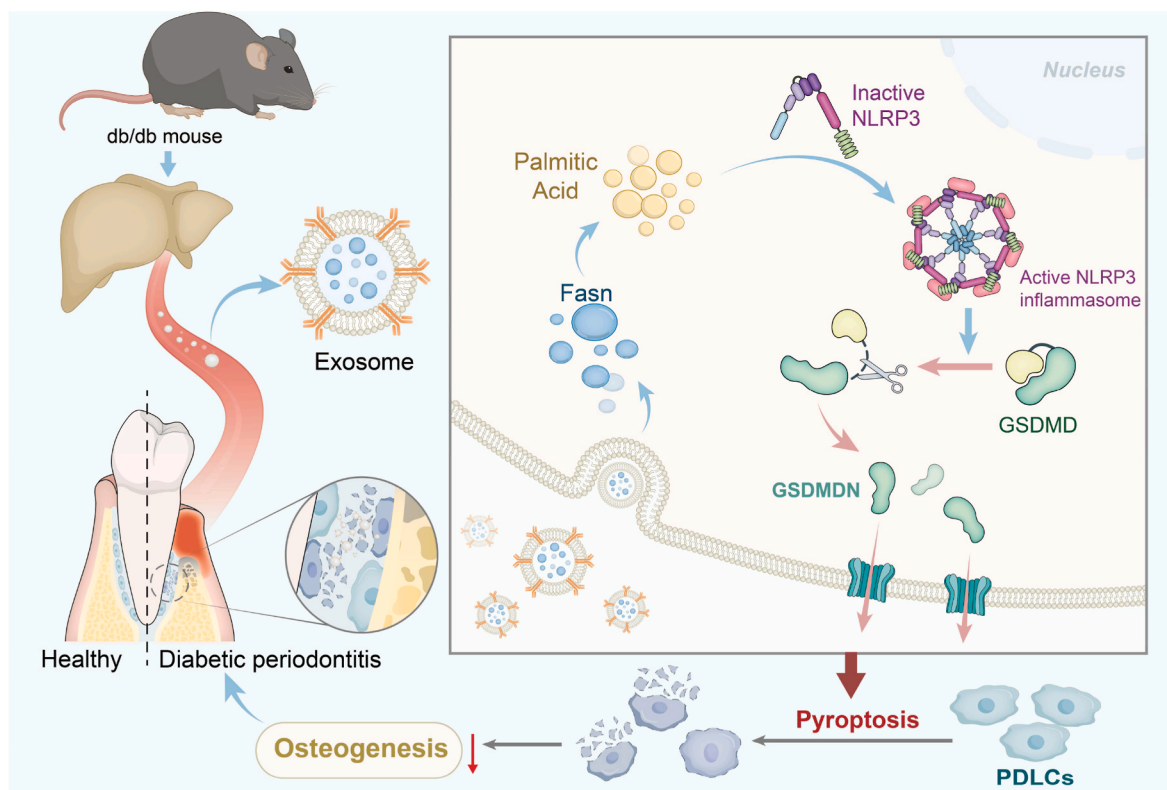
Fig. 7. Schematic illustration of the aggravated alveolar bone loss in type 2 diabetes mellitus caused by the Fasn-contained exosomes-induced pyroptosis.

should not exist via exosomes. Although fatty acids are essential for cell life, excess accumulation of fatty acids has been reported to cause pyroptosis, especially in extrahepatic tissue [55]. LC-MS reveals that palmitic acid (PA) was the principal product of Fasn in recipient PDLCs that has been reported to induce pyroptosis. Bone, an active part of metabolism and remodeling in the body, has been shown to be greatly influenced by metabolic and endocrine changes caused by diabetes [56]. The regeneration of diabetic bone defects remains challenging as the innate healing process is impaired by glucose fluctuation, reactive oxygen species, and overexpression of proteinases (such as matrix metalloproteinases, MMPs) [57,58]. Osteoporosis associated with diabetes have been confirmed the dysfunction on osteoblasts and osteoclasts, this study indicates a new mechanism by which changes in the lipid metabolism pathway of stem cells affect bone mass. In addition to excess ROS, inflammatory factors and advanced glycation end products (AGEs), the expression of heterotopic enzymes may provide a possible explanation for the incomplete recovery of alveolar ridge height only by glucose management and anti-inflammatory therapy [56,58]. Therefore, Fasn in liver serves as a novel therapeutic target for future engineering targeted strategy. More researches should be conducted on whether drugs targeting Fasn have a positive effect on diabetes-associated lesions.

This study innovatively demonstrated an ingenious design to track exosomes in vivo and identified the critical role of exosome in liver-bone axis communications. However, the precise mechanism governing exosome tropism remains elusive. Despite the well-recognized EVs-mediated organ communication, the pathways except for EVs need more explorations to better guide the development of clinical therapeutic strategies. Meanwhile, the expression of GSDMD-N or HMGB1 in non-CD90$^+$ cells was noticed, which requires us to further explore the role of other cells in this process. In addition, due to the lack of a specific marker for identification of mesenchymal stem cells (MSCs) in vivo, CD90 is widely used for MSC identification at present, including PDLCs in periodontal ligament [59]. It is also noticeable that the current experimental design for this study was limited to mice and cells derived from patients in consideration of ethical issues. Obtaining valuable periodontal tissue samples is challenging due to the difficulty in regenerating periodontal tissue and the inclusion of patients' teeth with typical diabetic periodontitis, which presents a significant obstacle in this field. Inclusion of the younger type 2 diabetic individuals in this study aimed to minimize the confounding influence of aging and other diabetic complications on the relationship between diabetes and periodontitis. Moreover, this study holds promise for identifying preventive strategies for these conditions at an earlier stage, which can have broader implications in clinical practice.

Overall, although there are still some limitations, this study provides new insights and lays a theoretical foundation for the follow-up researches. At present, the research mode based on organ communication promotes more studies to resolve existing clinical problems. In fact, the field under investigation is currently the subject of intense interest due to its promising prospects for clinical research and translational application. A variety of responsive materials integrating diagnosis and treatment regulate cell behavior for orchestrate of diabetic bone regeneration [60], which requires us to explore potent molecular targets or therapeutic strategies in the future to facilitate the development of clinical effective approaches.

5. Conclusions

In summary, we propose a new theory of exacerbated bone loss in diabetic periodontitis based on a better understanding of exosomes in systemic communication. The impaired liver in diabetes secretes plenty of abnormal exosomes into circulation, which are specifically distributed in the alveolar bone region and trigger the osteogenic dysfunction of PDLCs. Proteomic analysis reveals that fatty acid synthase transferred by liver-exosomes causes ectopic fatty acid synthesis, further inducing pyroptosis of PDLCs. This seminal discovery constructs an exosome-mediated communication bridge between the liver and bone to elucidate the previously unclear pathogenesis of diabetic periodontitis. Taken together, this study not only provide new perspectives for the study of diabetes-associated tissue regeneration disorders, but also pushing the recent advance on the tissue communication.

CRediT authorship contribution statement

Jiani Liu: Data curation, Formal analysis, Investigation, Validation, Writing – original draft. **Geng Dou:** Conceptualization, Formal analysis, Funding acquisition, Investigation, Writing – review & editing. **Wanmin Zhao:** Formal analysis, Investigation, Validation. **Ji'an Hu:** Methodology, Writing – review & editing. **Zhiwei Jiang:** Methodology, Writing – review & editing. **Wenzhe Wang:** Formal analysis, Software, Visualization. **Hanzhe Wang:** Formal analysis, Software, Visualization. **Shiyu Liu:** Project administration, Resources, Writing – review & editing. **Yan Jin:** Conceptualization, Project administration, Resources, Writing – review & editing. **Yimin Zhao:** Conceptualization, Project administration, Resources, Supervision, Writing – review & editing. **Qianming Chen:** Conceptualization, Funding acquisition, Project administration, Resources, Writing – review & editing. **Bei Li:** Conceptualization, Funding acquisition, Project administration, Resources, Writing – review & editing.

Declaration of competing interest

The authors declare that they have no known competing financial interests or personal relationships that could have appeared to influence the work reported in this paper.

Acknowledgements

Appendix A. Supplementary data

Supplementary data to this article can be found online at https://doi.org/10.1016/j.bioactmat.2023.10.022.

References

[1] R. Tevlin, et al., Pharmacological rescue of diabetic skeletal stem cell niches, Sci. Transl. Med. 9 (372) (2017).
[2] S. Maschalidi, et al., Targeting SLC7A11 improves efferocytosis by dendritic cells and wound healing in diabetes, Nature 606 (7915) (2022) 776–784.
[3] R. Liu, et al., Diabetes enhances periodontal bone loss through enhanced resorption and diminished bone formation, J. Dent. Res. 85 (6) (2006) 510–514.
[4] B.L. Pihlstrom, B.S. Michalowicz, N.W. Johnson, Periodontal diseases, Lancet 366 (9499) (2005) 1809–1820.
[5] E. Lalla, P.N. Papapanou, Diabetes mellitus and periodontitis: a tale of two common interrelated diseases, Nat. Rev. Endocrinol. 7 (12) (2011) 738–748.
[6] R.J. Genco, W.S. Borgnakke, Diabetes as a potential risk for periodontitis: association studies, Periodontol. 2000 83 (1) (2020) 40–45.
[7] B. Li, et al., SIRT6-regulated macrophage efferocytosis epigenetically controls inflammation resolution of diabetic periodontitis, Theranostics 13 (1) (2023) 231–249.
[8] P. Broz, P. Pelegrin, F. Shao, The gasdermins, a protein family executing cell death and inflammation, Nat. Rev. Immunol. 20 (3) (2020) 143–157.
[9] Q. Chen, et al., Periodontal inflammation-triggered by periodontal ligament stem cell pyroptosis exacerbates periodontitis, Front. Cell Dev. Biol. 9 (2021), 663037.
[10] M.B. Sordi, et al., Pyroptosis-mediated periodontal disease, Int. J. Mol. Sci. 23 (1) (2021).

[11] F. Liu, et al., USF2 enhances the osteogenic differentiation of PDLCs by promoting ATF4 transcriptional activities, J. Periodontal. Res. 55 (1) (2020) 68–76.

[12] D.W. Freeman, et al., Altered extracellular vesicle concentration, cargo, and function in diabetes, Diabetes 67 (11) (2018) 2377–2388.

[13] A. Brahmer, et al., Platelets, endothelial cells and leukocytes contribute to the exercise-triggered release of extracellular vesicles into the circulation, J. Extracell. Vesicles 8 (1) (2019), 1615820.

[14] N. Akbar, et al., Extracellular vesicles in metabolic disease, Diabetologia 62 (12) (2019) 2179–2187.

[15] G. Dou, et al., Chimeric apoptotic bodies functionalized with natural membrane and modular delivery system for inflammation modulation, Sci. Adv. 6 (30) (2020), eaba2987.

[16] S. Li, et al., Cell-derived microparticles in patients with type 2 diabetes mellitus: a systematic review and meta-analysis, Cell. Physiol. Biochem. 39 (6) (2016) 2439–2450.

[17] Y. Xiong, et al., Circulating exosomal miR-20b-5p inhibition restores Wnt9b signaling and reverses diabetes-associated impaired wound healing, Small 16 (3) (2020), e1904044.

[18] I. Huang-Doran, C.Y. Zhang, A. Vidal-Puig, Extracellular vesicles: novel mediators of cell communication in metabolic disease, Trends Endocrinol. Metabol. 28 (1) (2017) 3–18.

[19] W. Xia, et al., Damaged brain accelerates bone healing by releasing small extracellular vesicles that target osteoprogenitors, Nat. Commun. 12 (1) (2021) 6043.

[20] J. Wang, et al., Extracellular vesicles mediate the communication of adipose tissue with brain and promote cognitive impairment associated with insulin resistance, Cell Metabol. 34 (9) (2022) 1264–1279 e8.

[21] K. Lu, et al., Defects in a liver-bone axis contribute to hepatic osteodystrophy disease progression, Cell Metabol. 34 (3) (2022) 441–457 e7.

[22] P. Roman-Garcia, et al., Vitamin B(1)(2)-dependent taurine synthesis regulates growth and bone mass, J. Clin. Invest. 124 (7) (2014) 2988–3002.

[23] X. Wang, et al., A liver-bone endocrine relay by IGFBP1 promotes osteoclastogenesis and mediates FGF21-induced bone resorption, Cell Metabol. 22 (5) (2015) 811–824.

[24] S. Demir, et al., Emerging targets in type 2 diabetes and diabetic complications, Adv. Sci. 8 (18) (2021), e2100275.

[25] Y. Ji, et al., Hepatocyte-derived exosomes from early onset obese mice promote insulin sensitivity through miR-3075, Nat. Metab. 3 (9) (2021) 1163–1174.

[26] F. Jiang, et al., Hepatocyte-derived extracellular vesicles promote endothelial inflammation and atherogenesis via microRNA-1, J. Hepatol. 72 (1) (2020) 156–166.

[27] Y. Chao, et al., The role of miRNAs carried by extracellular vesicles in type 2 diabetes and its complications, J. Diabetes. 15 (10) (2023) 838–852.

[28] Y. Qin, et al., Whole-transcriptome analysis of serum L1CAM-captured extracellular vesicles reveals neural and glycosylation changes in autism spectrum disorder, J. Mol. Neurosci. 72 (6) (2022) 1274–1292.

[29] R. Crescitelli, C. Lasser, J. Lotvall, Isolation and characterization of extracellular vesicle subpopulations from tissues, Nat. Protoc. 16 (3) (2021) 1548–1580.

[30] E. Willms, et al., Cells release subpopulations of exosomes with distinct molecular and biological properties, Sci. Rep. 6 (2016), 22519.

[31] Y. Hu, et al., Fatty acid synthase-suppressor screening identifies sorting nexin 8 as a therapeutic target for NAFLD, Hepatology 74 (5) (2021) 2508–2525.

[32] J. Marchesan, et al., An experimental murine model to study periodontitis, Nat. Protoc. 13 (10) (2018) 2247–2267.

[33] B.M. Seo, et al., Investigation of multipotent postnatal stem cells from human periodontal ligament, Lancet 364 (9429) (2004) 149–155.

[34] J. Shi, et al., Cleavage of GSDMD by inflammatory caspases determines pyroptotic cell death, Nature 526 (7575) (2015) 660–665.

[35] P. Zhao, et al., Hyperglycaemia-associated macrophage pyroptosis accelerates periodontal inflamm-aging, J. Clin. Periodontol. 48 (10) (2021) 1379–1392.

[36] N. Noren Hooten, M.K. Evans, Extracellular vesicles as signaling mediators in type 2 diabetes mellitus, Am. J. Physiol. Cell Physiol. 318 (6) (2020) C1189–C1199.

[37] C. Castano, et al., Obesity-associated exosomal miRNAs modulate glucose and lipid metabolism in mice, Proc. Natl. Acad. Sci. U.S.A. 115 (48) (2018) 12158–12163.

[38] K. Essandoh, et al., Blockade of exosome generation with GW4869 dampens the sepsis-induced inflammation and cardiac dysfunction, Biochim. Biophys. Acta 1852 (11) (2015) 2362–2371.

[39] Q. Zhai, et al., Nanorepairers rescue inflammation-induced mitochondrial dysfunction in mesenchymal stem cells, Adv. Sci. 9 (4) (2022), e2103839.

[40] S. Eid, et al., New insights into the mechanisms of diabetic complications: role of lipids and lipid metabolism, Diabetologia 62 (9) (2019) 1539–1549.

[41] I.J. Lodhi, et al., Inhibiting adipose tissue lipogenesis reprograms thermogenesis and PPARgamma activation to decrease diet-induced obesity, Cell Metabol. 16 (2) (2012) 189–201.

[42] D. Dasgupta, et al., IRE1A stimulates hepatocyte-derived extracellular vesicles that promote inflammation in mice with steatohepatitis, Gastroenterology 159 (4) (2020) 1487–1503 e17.

[43] M. Poggio, et al., Suppression of exosomal PD-L1 induces systemic anti-tumor immunity and memory, Cell 177 (2) (2019) 414–427 e13.

[44] R. Kawata, et al., Macrophage-derived extracellular vesicles regulate concanavalin A-induced hepatitis by suppressing macrophage cytokine production, Toxicology 443 (2020), 152544.

[45] M.Q. Yang, et al., Interferon regulatory factor 1-Rab27a regulated extracellular vesicles promote liver ischemia/reperfusion injury, Hepatology 67 (3) (2018) 1056–1070.

[46] Z. Zhaolin, et al., Role of pyroptosis in cardiovascular disease, Cell Prolif. 52 (2) (2019), e12563.

[47] X. Zeng, et al., Oleic acid ameliorates palmitic acid induced hepatocellular lipotoxicity by inhibition of ER stress and pyroptosis, Nutr. Metab. 17 (2020) 11.

[48] H. Wen, et al., Fatty acid-induced NLRP3-ASC inflammasome activation interferes with insulin signaling, Nat. Immunol. 12 (5) (2011) 408–415.

[49] R.S. de Molon, et al., Impact of diabetes mellitus and metabolic control on bone healing around osseointegrated implants: removal torque and histomorphometric analysis in rats, Clin. Oral Implants Res. 24 (7) (2013) 831–837.

[50] T. Kocher, et al., Periodontal complications of hyperglycemia/diabetes mellitus: epidemiologic complexity and clinical challenge, Periodontol. 2000 78 (1) (2018) 59–97.

[51] S. Ehnert, et al., Hepatic osteodystrophy-molecular mechanisms proposed to favor its development, Int. J. Mol. Sci. 20 (10) (2019).

[52] A.K. Nussler, et al., Chronic CCl4 intoxication causes liver and bone damage similar to the human pathology of hepatic osteodystrophy: a mouse model to analyse the liver-bone axis, Arch. Toxicol. 88 (4) (2014) 997–1006.

[53] F. Wang, et al., Circulating small extracellular vesicles from patients with periodontitis contribute to development of insulin resistance, J. Periodontol. 93 (12) (2022) 1902–1915.

[54] J. Zhou, et al., Pyroptosis and degenerative diseases of the elderly, Cell Death Dis. 14 (2) (2023) 94.

[55] N. Pizato, et al., Omega-3 docosahexaenoic acid induces pyroptosis cell death in triple-negative breast cancer cells, Sci. Rep. 8 (1) (2018) 1952.

[56] Y.Y. Wu, E. Xiao, D.T. Graves, Diabetes mellitus related bone metabolism and periodontal disease, Int. J. Oral Sci. 7 (2) (2015) 63–72.

[57] D. Li, et al., A logic-based diagnostic and therapeutic hydrogel with multistimuli responsiveness to orchestrate diabetic bone regeneration, Adv. Mater. 34 (11) (2022), e2108430.

[58] L. Xin, et al., Four-Octyl itaconate ameliorates periodontal destruction via Nrf2-dependent antioxidant system, Int. J. Oral Sci. 14 (1) (2022) 27.

[59] S. Aydin, F. Sahin, Stem cells derived from dental tissues, Adv. Exp. Med. Biol. 1144 (2019) 123–132.

[60] Q. He, et al., Safeguarding osteointegration in diabetic patients: a potent "Chain Armor" Coating for scavenging ROS and macrophage reprogramming in a microenvironment-responsive manner, Adv. Funct. Mater. 31 (31) (2021), 2101611.